

Contrast sensitive fiber optic Michelson interferometer as elongation sensor

M. SZUSTAKOWSKI* and N. PAŁKA

Institute of Optoelectronics, Military University of Technology
2 Kaliskiego Str., 00-908 Warsaw, Poland

Theoretical description of a contrast phenomenon in an unbalanced fiber optic Michelson's interferometer with a multimode laser is shown. Required characteristic features of the contrast function for an elongation sensor are determined. Optimal spectrum for the dislocation sensor is calculated theoretically. A laser which parameters fulfilled the requirements was found. The elongation sensor based on contrast oscillations in an unbalanced fiber optic Michelson interferometer with a 3×3 coupler is described. Direct contrast-sensitive elongation measurement range limited to 200- μm long slope is expanded up to 5 mm by means of contrast oscillations linearization scheme. Elongation modulator in a reference arm of the interferometer is used. Experimental setup, signal processing scheme and software were worked out. For 1-m long sensor, the 5-mm measuring range with 28- μm uncertainty was obtained.

Keywords: fiber optic, Michelson interferometer, contrast function, elongation sensor.

1. Introduction

Civil structure monitoring is a fundamental task to guarantee the safety of a structure and its users. Information about a structure helps planning maintenance, increases the knowledge about its real behaviour and permits optimisation of future structures. In recent years, fiber optic sensors are gaining in importance in this field and they are an ideal choice for many applications. Optical sensors have such advantages as high elongation sensitivity, immunity to electromagnetic disturbance and lightweight. In many applications, optical fiber can compete with mature electronic technologies. Elongation of a fiber optic is limited by its ultimate strain that is equal to 2–3% [1].

A few fiber optic sensors used for dislocation measurements are known. Generally, when light propagates through a lightguide, it is sensitive to lots of internal and external factors. Operation of the most known sensors is based on fiber Bragg gratings (FBG's) [2,4] and interferometers, both coherence [1] and white light [3].

According to statistics [4], fiber Bragg gratings are the most widely studied topics today. The fiber Bragg grating is an element in a fiber optic core with a periodic modulation of the refractive index. From the broad incident light spectrum, gratings reflect a specific wavelength that depends on their strain and temperature. An interrogation unit extracts information from the light signals coming from the sensor head.

Fiber optic interferometer elongation sensors can work in Michelson's [5], Mach-Zehnder's [6], and Fabry-Perot's [1,7] configurations. Due to their sensitivity, they have attracted attention of researches for years. Interference can be only observed if a basic condition is fulfilled, i.e., an optical path difference within the interferometer is shorter than a coherence length of a source that is used to illuminate the interferometer.

The coherence light interferometers are based on the measurement of a phase difference between two light beams, while one of it is subjected to a measurand, an optical path elongation in this case. An output irradiance observable at detectors is an implicit function of the phase difference. A few special signal processing schemes known as demodulation are exploited to recover the phase information [6]. Additionally, to increase a measuring range beyond an optical path length difference of 2π rad range a fringe counter is needed. The demodulation schemes require the contrast to be constant and nearly equal to 1, what can be fulfilled for single-mode semiconductor lasers in the limited range of a few dozen of millimetres [7].

The white light technique makes use of two interferometers in tandem configuration. A low-coherence source illuminates an unbalanced sensing interferometer which is interrogated by a local receiving interferometer. The path imbalance in the sensing interferometer is greater than the coherence length of the source, so that to view interference fringes the receiving interferometer path imbalance must match that of the sensing interferometer. A path length change in the sensor is tracked by the receiver [8].

* e-mail: mszustakowski@wat.edu.pl

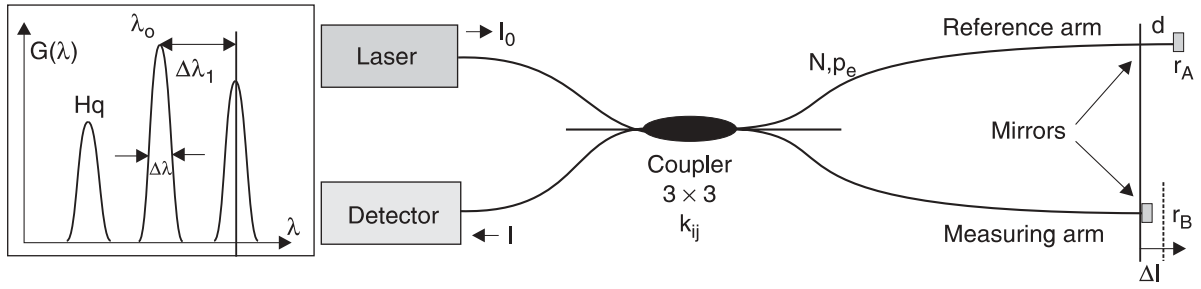


Fig. 1. Diagram of the unbalanced fiber optic Michelson interferometer with symbols of source spectrum parameters.

We propose a competitive method, which exploits the contrast phenomenon in the unbalanced Michelson interferometer. The contrast describes the amplitude of the interference output irradiance and derives from a source spectrum. If a specially selected few longitudinal-modes-laser is used as the illuminating source, the contrast oscillates as a function of one arm elongation. Taking advantage of a special signal processing scheme, the elongation measurement is possible.

The resolution of the contrast-based method is worse than the phase-based method. However, for number of applications, e.g., monitoring of civil engineering structures, submicrometer resolution is not required and a few dozen of micrometers is acceptable.

2. Theory

A diagram of the unbalanced fiber optic Michelson interferometer is presented in Fig. 1 [8]. Light from the source is coupled into a monomode fiber and amplitude is divided into measuring and reference arms by a 3×3 coupler. Two guided beams are reflected by the mirrors, recombine again and mix coherently to produce interference observable at the output. We assume that state of polarization of the guided beam remains unchanged throughout.

The irradiance observed at the detector, as the function of elongation of measuring arm Δl , can be written as [8]

$$I(\Delta l) = I_0 (k_{12}^2 k_{22}^2 r_A^2 + k_{13}^2 k_{32}^2 r_B^2) \times \left[1 + V(\Delta l) \cos \left(2 \frac{2\pi}{\lambda_0} N [d - \Delta l(1 - p_e)] \right) \right] \quad (1)$$

where V is the contrast of the interferometer, d is the arms length difference, I_0 is the source irradiance, N is the effective refractive index of a fiber, λ_0 is the wavelength, $p_e = 0.22$ is the effective photoelastic coefficient of a fiber, k_{ij} are the amplitude coefficients of the coupler, and r_A and r_B are the reflection coefficients of the mirrors. We assumed that elongation does not change the polarization state of the guided beam in the arms of interferometer [9].

Basing on the correlation Goodman's analysis [10], for the Gaussian distribution of each mode, we obtained the relationship between the interferometer contrast, the source spectrum presented in Fig. 1 and fiber optic parameters as a

function of the elongation Δl of the measuring arm in a wavelength domain

$$V(\Delta l) = \frac{k_{12} k_{22} r_A k_{13} k_{32} r_B}{k_{12}^2 k_{22}^2 r_A^2 + k_{13}^2 k_{32}^2 r_B^2} \left(\sum_{q=1}^p H_q \right)^{-1} \times \exp \left[- \left(\frac{\pi N}{\sqrt{\ln 2}} \frac{\Delta \lambda}{\lambda_0^2} [d - \Delta l(1 - p_e)] \right)^2 \right] \quad (2a)$$

$$\times \sqrt{\left(\sum_{q=1}^p H_q \cos(A) \right)^2 + \left(\sum_{q=1}^p H_q \sin(A) \right)^2}, \quad (2b)$$

$$A = 4\pi \frac{\Delta \lambda_1}{\lambda_0^2} (q-1) N [d - \Delta l(1 - p_e)],$$

where λ_0 is the wavelength, $\Delta \lambda$ is the spectral halfwidth, $\Delta \lambda_1$ is the mode spacing, H_q is the amplitude of the q^{th} laser mode, and d is the initial interferometer arms length difference.

One mode gives the exponential dependence, while for multimode lasers the contrast oscillates within the envelope determined by one mode contrast dependence. It can be seen, that when a number of laser modes increases, the higher gradient of slope is observed [11].

3. Conception of contrastometric dislocation sensor

The contrast functions $V(\Delta l)$ depends on elongation of the measuring arm of the interferometer, so construction of an elongation sensor can be based on this phenomenon. The presented solution is similar to interferometer signal demodulation schemes, e.g., digital inverse trigonometric [6] and differentiation and cross multiplication [11], where a 120° phase shift of the output signals, caused by the 3×3, coupler is exploited.

A diagram of the proposed contrast-based sensor is schematically presented in Fig. 2. This sensor requires the contrast function to be triangular (Fig. 3) what imposes application of a source of the interferometer determined in the next section. This source through its contrast function guarantees correctness of the presented algorithm. Periodic character of the contrast function reduces useful measuring range to one slope. To overcome this problem, linearization of contrast oscillations scheme is proposed.

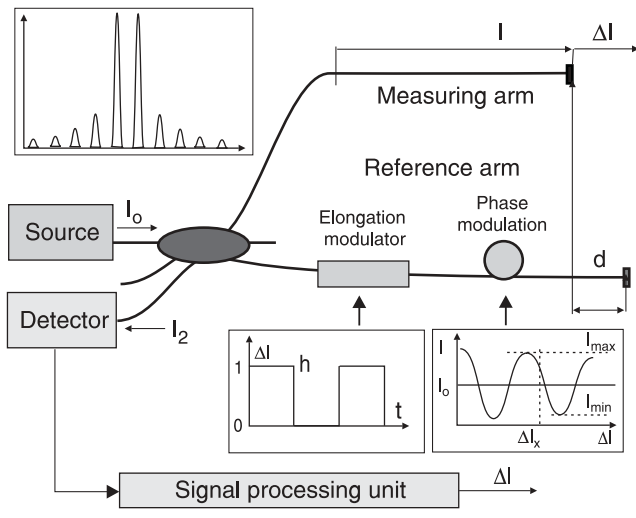


Fig. 2. Diagram of the contrast-based elongation sensor.

During measurement, the interferometer arm is elongated and shortened so contrast slopes changes are accidental. Making use of only one contrast function (V_0) leads to ambiguity in minima and maxima. In this connection, we propose to place the elongation modulator into the reference arm of the interferometer (Fig. 2). This modulator, driven rectangular function, causes periodical fixed change of the reference arm length (shift). In every the i^{th} modulation period, two values of the contrast are obtained, i.e., $v0(i)$ and $v1(i)$. As a result, two shifted contrast functions V_0 and V_1 are created (Fig. 3). The V_0 is exploited for linearization while V_1 is necessary for slope determination (a dotted line in Fig. 3).

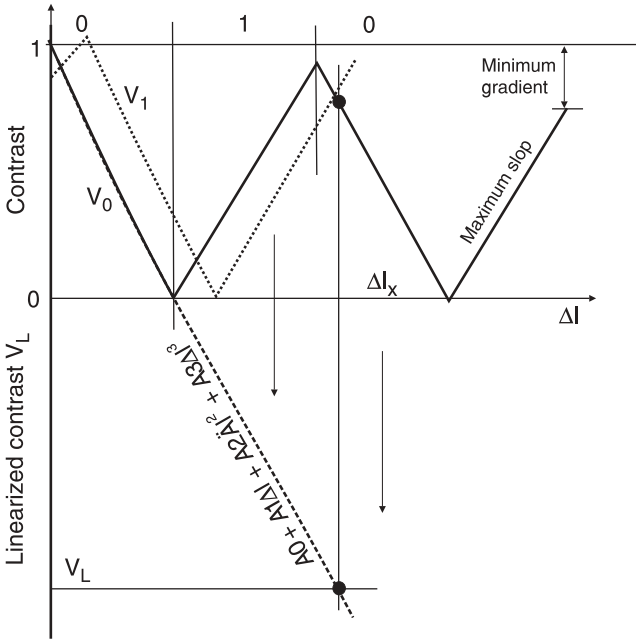


Fig. 3. Contrast linearisation scheme. Optimal contrast function features.

These two contrast functions determine the slope of V_0 without ambiguity. The contrast V_0 elongation range can be divided into the decreasing zone (0) and the increasing zone (1) basing on the relations (Fig. 3)

zone (0)

$$v1(i) > 0.5 \text{ and } v0(i) \geq v1(i) \text{ and } \left(\begin{matrix} v0(i-1) > v0(i) & v0(i-1) < v0(i) \\ v1(i-1) < v1(i) & \text{or } v1(i-1) > v1(i) \end{matrix} \right) \tag{3}$$

or

$$v0(i) < v1(i) \text{ and } \left(\begin{matrix} v0(i-1) > v0(i) & v0(i-1) < v0(i) \\ v1(i-1) > v1(i) & \text{or } v1(i-1) < v1(i) \end{matrix} \right) \tag{4}$$

zone (1)

$$v1(i) > 0.5 \text{ and } v0(i) < v1(i) \text{ and } \left(\begin{matrix} v0(i-1) > v0(i) & v0(i-1) < v0(i) \\ v1(i-1) < v1(i) & \text{or } v1(i-1) > v1(i) \end{matrix} \right) \tag{5}$$

or

$$v0(i) > v1(i) \text{ and } \left(\begin{matrix} v0(i-1) > v0(i) & v0(i-1) < v0(i) \\ v1(i-1) > v1(i) & \text{or } v1(i-1) < v1(i) \end{matrix} \right) \tag{6}$$

The determined zones are exploited for linearization of contrast oscillations during elongation measurement according to the following algorithm. The algorithm starts with $i = 1, w = 0$ and the measured values of contrast $v0(i), v1(i), v0(i-1), v1(i-1)$ on the first (0) zone slope. For each contrast value $v0(i)$, a linearized contrast value $v_L(i)$ is calculated. If the current zone slope is equal to 0 (nonascending) to obtain $v_L(i)$, the current value of w is subtracted from $v0(i)$. Otherwise, $v_L(i)$ is determined by means of the previous linearized contrast value $v_L(i-1)$ and the difference between current $v0(i)$ and previous $v0(i-1)$ values.

All v_L values are located on the 3rd degree polynomial reference curve which coefficients ($A0$ – $A3$) were determined earlier. The linearized contrast values v_L is next substituted to the equation

$$v_L = A0 + A1\Delta l_x + A2\Delta l_x^2 + A3\Delta l_x^3 \tag{7}$$

and the elongation value Δl_x is calculated numerically.

During the reference measurement, the interferometer is elongated with a constant step. Simultaneously, the obtained contrast values are linearized (unbent) according to the scheme shown in Fig. 3. These linearized contrast values are next fitted with the 3rd degree polynomial. The approximation coefficients A_0 – A_3 constitute the reference curve and they are stored in memory. The degree of polynomial was found experimentally.

Contrast measurement in the Michelson interferometer requires a phase modulator situated in the reference arm (Fig. 2). This device causes a periodical modulation of the cosine term in Eq. 1 what makes it possible to measure the maximum I_{\max} and minimum I_{\min} value of the irradiance in the closest vicinity of the elongation state Δl and to calculate the contrast according to a relation [8]

$$V(\Delta l) = \frac{I_{\max} - I_{\min}}{I_{\max} + I_{\min}}. \quad (8)$$

4. Choice of elements

In the present section, theoretical analysis of source spectrum and interferometer arm lengths is carried out in order to determine their optimal parameters.

4.1. Source spectrum parameters

The above presented algorithm of linearization requires the contrast function to be triangular. We determined additional contrast features desirable for the sensor and came to the conclusion that the optimum contrast function should have: maximum slope (maximum sensitivity) and minimum gradient of the whole contrast function (Fig. 3). On this basis we examined the source parameters: halfwidth, mode spacing, and wavelength. The conclusions are: halfwidth value should be as lower as possible, mode spacing value should be as higher as possible, both wavelengths (1.3 μm and 1.55 μm) can be equally applied [11].

Two methods were used to determine the amplitudes of modes of the source power density distribution $[G_{opt}(\lambda)]$ that ensures the required contrast function.

First, the amplitudes were calculated by means of the Fourier spectroscopy method [13]. Unfortunately, in this approach we obtained unequal mode spacing values what prevented us from searching for such a source.

So, another variational method was proposed to determine this spectrum. For calculation we assumed laser parameters similar to the lasers we possessed: $\lambda_0 = 1.275 \mu\text{m}$, $\Delta\lambda = 70 \text{ pm}$, $\Delta\lambda_1 = 1.1 \text{ nm}$ and $p = 10$ modes. Every mode amplitude (H_q) lay between 0 and 1. For every combination of the laser mode amplitudes we determined the contrast function limited to one slope. For this curve we calculated sensitivity, the slope of a straight line (a) by means of the least squares method and linearity by the Pearson coefficient R^2 . The maximum sensitivity $a = -2.836 \text{ mm}^{-1}$ and linearity $R^2 = 0.9991$ were obtained for the following amplitudes

$$H = \{0.009, 0.012, 0.044, 0.100, 1.000, 1.000, 0.100, 0.045, 0.012, 0.009\}.$$

Spectra of 10 semiconductor Holotex POM lasers were measured and their parameters were determined. The laser POM-14-1, which parameters were the most similar to the calculated above, was selected to further research. The detected spectrum of the laser is shown in Fig. 4. We fit every q^{th} mode with Gaussian distribution. Good agreement between the measured values and the approximations proved correctness of the assumed Gaussian distribution for the earlier contrast calculation [Eq. (2)]. From the approximations, we determined parameters of the Holotex POM-14-1 laser:

- amplitudes of modes which are equal to $H^2 = \{0.0065, 0.0105, 0.0384, 0.0752, 0.9631, 1.0000, 0.0842, 0.0311, 0.0127, 0.0087\}$,
- mean mode spacing and its standard deviation: $\overline{\Delta\lambda_1} = 1105 \pm 56 \text{ pm}$
- mean halfwidth and its standard deviation: $\overline{\Delta\lambda} = 67 \pm 2 \text{ pm}$
- wavelength $\lambda_0 = 1.27553 \mu\text{m}$

Figure 5 presents three diagrams of contrast function:

- optimal, calculated by means of Eq. (2) for $\Delta\lambda_0$, $\Delta\lambda$, $\Delta\lambda_1$ and H^1 ,
- calculated for the measured parameters of the used POM-14-1 laser λ_0 , $\Delta\lambda_1$, $\Delta\lambda$ and H^2 ,
- measured at an interferometer arrangement with the Holotex POM-14-1 laser. The arrangement is described in Sec. 5.

We can see that these diagrams are very similar with regards to the shape and values, what proved correctness of the calculations. Small differences at the bottom part of the figure are derived from the fact that in the measured and calculated cases the values of amplitudes were not symmetrical what is a condition that the contrast reaches zero. This condition was fulfilled in the optimal case.

The initial part of the measured contrast function is derived from the fact that the fiber optic in the measuring arm was not elongated despite the stepping motor movement. Proper elongation starts for about 0.2 mm. A zero path dif-

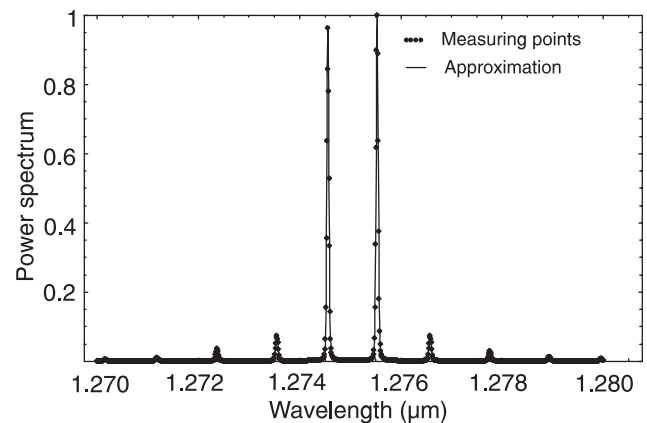


Fig. 4. Detected spectrum of the POM-14-1 Holotex laser.

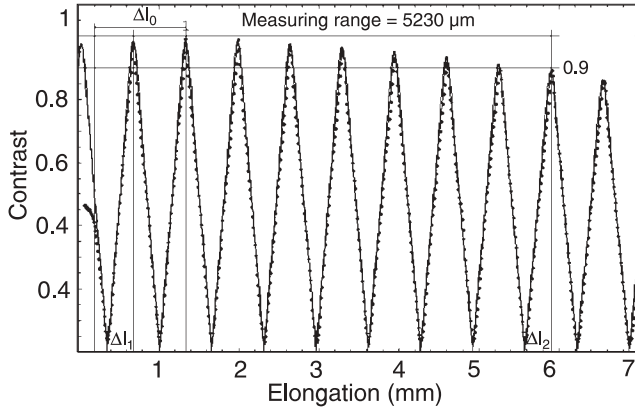


Fig. 5. Contrast functions: optimal (grey), calculated (black) and measured (dots).

ference elongation (maximum peak value) is obtained for 1.34-mm elongation. A difference between the above values $\Delta\lambda_0$ is equal to about 1.14 mm. So, the arm length difference d_{meas} can be determined from Eq. (2a) as

$$d_{meas} = \Delta\lambda_0(1 - p_e) \cong 0.89 \text{ mm} \quad (9)$$

The value of d_{meas} is similar to the directly measured arms length difference that is equal to 1 mm. We think that discrepancy results from insufficient resolution of the second measurement.

The measured contrast function is very similar to the optimal ones, so the found Holotex laser can be used as a source for the designed sensor.

4.2. Interferometer arm lengths and measuring range

Within an elastic limit, the contrast value V_{th} is proposed as a threshold for elongation. Below that value, the contrast function fall causes decrease in sensor sensitivity (Fig. 6). Basing on Eq. (2), the maximum elongation range L_{max} can be written as

$$L_{max} = 2 \frac{\sqrt{-\ln 2 \ln(V_{th})} \lambda_0^2}{(1 - p_e) \pi N} \frac{1}{\Delta\lambda} \quad (10)$$

where V_{th} is the contrast threshold.

An optimal difference of the interferometer arm d_{opt} that supports L_{max} can be expressed as

$$d_{opt} = \frac{\sqrt{-\ln 2 \ln(V_{th})} \lambda_0^2}{\pi N} \frac{1}{\Delta\lambda}. \quad (11)$$

It is clear, that the reference arm in the designed sensor should be longer than the measuring arm. Figure 7 presents the elongation range L_{max} and the optimal arms difference d_{opt} as a function of the laser halfwidth for $N = 1.464$, $\lambda_0 = 1275.5 \text{ nm}$ and $V_{th} = 0.9$.

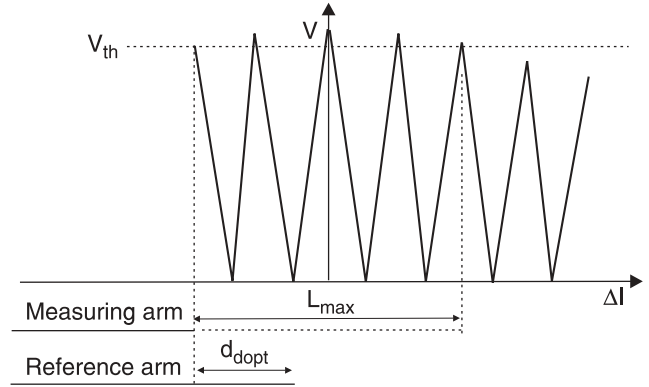


Fig. 6. The elongation range (L_{max}) and the optimal arms difference (d_{opt}) idea.

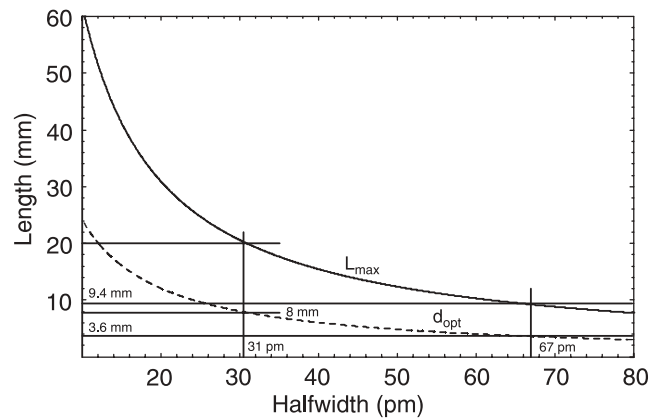


Fig. 7. The elongation range (L_{max} – solid) and the optimal arms difference (d_{opt} – dashed) versus the laser halfwidth.

The presented formulas make it possible to select optimal parameters of elements for required sensors features. For example, for a 20-mm measuring range a 31-pm halfwidth laser and an 8-mm arms length difference is needed ($V_{th} = 0.9$).

5. Sensor arrangement

In order to prove the sensor proper operation and theoretically estimate its parameters, a simulation model in the LabView was built and tested. The parameters of real elements were used for simulations. The obtained parameters of 1-m long sensor, 5-mm measuring range and 12- μm uncertainty allow us to construct the real sensor [14].

Next, a laboratory model of the sensor – the unbalanced Michelson interferometer setup with the modulators was built and tested on a specially designed measuring position in order to evaluate its parameters (Fig. 8). Research was carried out at the stable temperature conditions $22^\circ\text{C} \pm 1^\circ\text{C}$. As the source of the interferometer, the 1.3- μm Holotex POM-14-1 semiconductor laser was used, the spectrum of which is shown in Fig. 4. In order to avoid mode hopping, the polarization-independent isolator with 42 dB was applied. We exploited the 3 \times 3 coupler made by Gould with

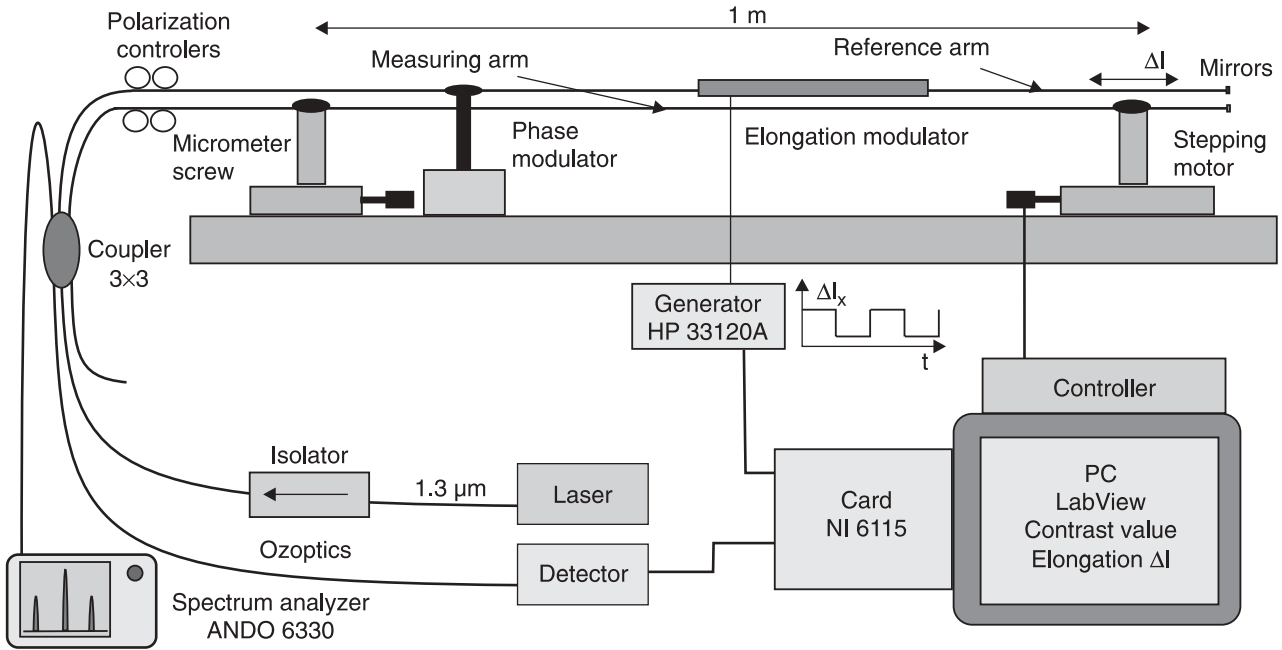


Fig. 8. Experimental arrangement.

the measuring L_A and reference L_B arm length equal to 200.9 cm and 201.0 cm, respectively. The arms length difference $d = 1$ mm. There is no fusion splices along the arms in order to avoid accidental reflections and decreasing in performance. The arm ends are covered with 200- μ m layer of gold to assure high reflection. The measuring arm is fixed to two handles of optical bench at the distance of one meter, while the reference arm is nearby. Temperature fluctuations equally affect both arms, so their length difference remains constant what makes this sensor insensitive to external perturbations. One of the handles is moved by a PC-controlled stepping motor in order to elongate the measuring arm during reference measurements. The second handle is moved by a Mitutoyo micrometer screw with 1- μ m resolution and 2- μ m accuracy to ensure better resolution during elongation measurements.

Ando 6330 spectrum analyser controls the laser spectrum. Polarization controllers in both arms of the interferometer ensure equivalent states of polarization of the recombining beams. HP-33120A generator controls modulation frequency of the elongation modulator. The phase modulator, situated in the reference arm, is made out of a piezoelectric cylinder with six turns of fiber wrapped around it. The applied voltage is fitted in order to obtain the required amplitude of modulation. The modulation frequency of 13.4 kHz results from the acoustic resonance frequency of the cylinder.

During a measurement of the reference curve, the elongation modulator is switched off and the stepping motor elongates the sensor with 10- μ m step. For every state of the elongation Δl , 10 scans (acquisition points) are collected. Maximum and minimum values of the scan are determined and by means of Eq. (8) the contrast value is calculated. The averaged values of the contrast are next linearised. The

obtained data are fitted with the 3rd degree polynomial and approximation coefficients A_0 – A_3 are stored.

During the elongation measurement, the elongation modulator is on. Theoretical signal from the photodetector during elongation and elongation modulator periods are plotted in Fig. 9(a). For every the i^{th} modulation period, contrast values are determined and averaged as above, separately for 0 and 1 state of the modulator [Fig. 9(b)]. Consequently, the contrast values $v_0(i)$ and $v_1(i)$ are obtained [Fig. 9(c)]. Basing on Eqs. (3–6), the zones can be determined. Next, by means of the algorithm presented in Sec. 3, the linearised contrast value $v_L(i)$ is calculated and substituted to Eq. (7). The elongation value $\Delta l_x(i)$ is a numeri-

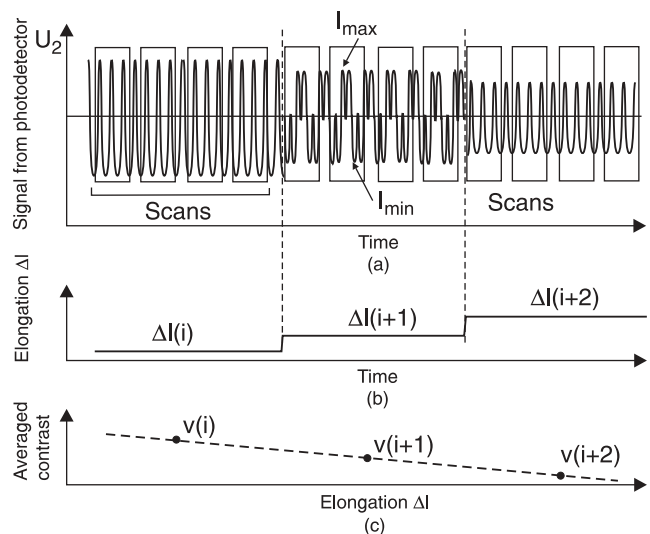


Fig. 9. Signal processing diagram of elongation measurement: theoretical signal from the photodetector (a), state of the elongation modulator (b), and contrast values v_0 and v_1 (c).

cal solution of Eq. (7). We assumed 1- μm resolution of the presented Δl_x value.

The signals from detector are collected by the National Instruments NI-6115 acquisition card and processed by the LabView program, which also controls the measurement as well as visualizes and stores the data.

6. Elongation measurements

Research was undertaken for determination of the sensor's parameters and evaluation of its practical usefulness. Part of the measured contrast function (Fig. 5) was exploited for the sensor, from elongation equal to $\Delta l_1 = 680 \mu\text{m}$ what corresponds to the first peak and up to $\Delta l_2 = 5910 \mu\text{m}$ (limit for $V_{th} = 0.9$). So, the useful elongation range is $5230 \mu\text{m}$.

In a reference measurement, conducted according to the algorithm presented in Sec. 5, the approximation coefficients have been calculated and they are as follows: $A_0 = 0.959$, $A_1 = -2.895 \times 10^{-3} \mu\text{m}^{-1}$, $A_2 = -7.204 \times 10^{-9} \mu\text{m}^{-2}$, and $A_3 = 5.051 \times 10^{-12} \mu\text{m}^{-3}$. The second handle, moving with the micrometer screw, was exploited in further research because of the higher accuracy. From the 0–5000 μm elongation range $n = 10$ points (Δl^j) were chosen, every 500 μm starts from 500 μm (500 μm ... 5000 μm). The measuring arm of the interferometer was $m = 10$ times elongated and the sensor indications (Δl_X^{jq}) were stored for the chosen points. Next, the collected data were averaged for the appropriate points (Δl_X^j) and their standard deviations $S(\Delta l_X^j)$ were also calculated. The obtained values are plotted in Fig. 9.

In order to estimate an uncertainty of the elongation measurement, we took advantage of the correction coefficient method [15]. The correction coefficient (CF_b) can be calculated from a formula

$$CF_b = \frac{1}{n} \sum_{j=1}^n \frac{\Delta l^j}{\Delta l_X^j}, \quad (12)$$

and it is equal to 0.999. The expanded uncertainty in the every j^{th} measuring point was calculated as [15]

$$U^j = CM \sqrt{(u_{BMB})^2 + \frac{\sum_{q=1}^m \left(\Delta l_X^{jq} - \frac{\Delta l_X^j}{CF_b} \right)^2}{n-1}}, \quad (13)$$

where $CM = 2$ is the expansion coefficient and u_{BMB} is the B type uncertainty of the examined sensor what is equal to its resolution divided by $\sqrt{3}$. The values of U^j are graphed in Fig. 10. The maximum value of the expanded uncertainty equal to 28 μm is the uncertainty of the examined sensor.

The sensor was also tested for elongations and shortenings with equal step (20 μm and 50 μm) what is

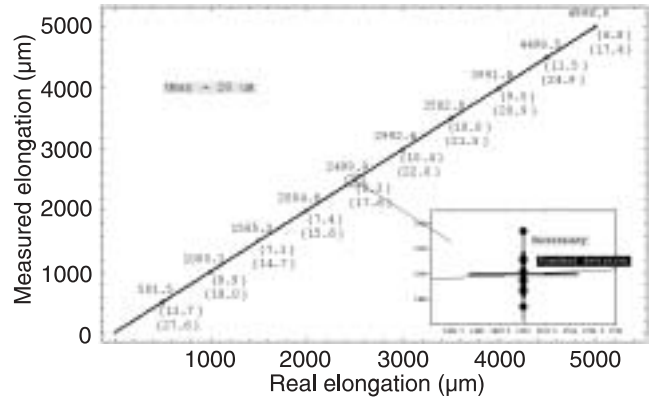


Fig. 10. Experimental results of elongation measurement. For every point value of averaged elongation, standard deviation and expanded uncertainty is presented from top to bottom. Figure inside shows enlargement for 2500 μm region, where horizontal line is uncertainty of the micrometer screw.

shown in Figs. 11(a) and 11(b), respectively. For both cases the results are satisfactory. The measured values oscillate within the $\pm 5 \mu\text{m}$ range around the real elongation value.

7. Conclusions

In this paper, the experimental results of the contrast-based elongation sensor were presented. For 1-m long sensor, the 5-mm measuring range with 28- μm uncertainty was obtained. As far as the sensor's arm lengths are concerned, they can be increased up to a few dozen meters, because only the arms length difference is important from the prin-

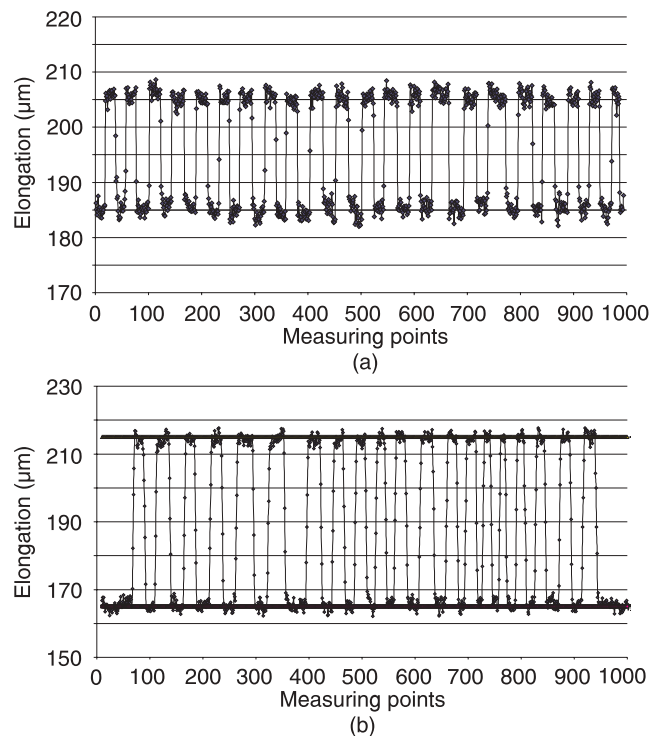


Fig. 11. Elongations and shortenings with equal step: 20 μm (a) and 50 μm (b).

principle of operation viewpoint. The elongation range depends on the arms difference and the halfwidth of the light source. If a laser with smaller value of a halfwidth is used, the elongation range can be expanded up to ultimate limit of the used fiber, which is equal to about 2%.

The uncertainty value results from small fluctuations of laser mode amplitudes and the fact that the used laser spectrum was similar, but not equal to the optimal one. It is clear that crucial issue to this sensor is stability of a laser spectrum because every change of it causes also the contrast changes. We consider application a solid-state microchip laser that seems to have more stable parameters than semiconductor lasers. Another source of uncertainty is the elongation modulator instability. The proposed linearisation processing scheme decreases also performance because of nonlinearity of the reference curve.

The sensor research was conducted at a constant temperature. For proper operation at changing temperatures, the modulators cannot influence on the reference arm length or this influence has to be compensated.

The sensor frequency is equal to 1 Hz what was derived from operation of the elongation modulator. We also consider application of a modulator that includes a function of the phase and elongation modulation. This solution should increase the frequency and improve the sensor stability.

The measured parameters of the sensor are similar to the parameters achieved by commercially available electric-based sensors as well as fiber optic ones. However, we believe that application of better elements improves the sensor performance.

This fact allows us foreseeing of potential usefulness of the contrast-sensitive Michelson interferometer-based sensor. We predict application of the elongation sensor to monitor the state of civil engineering structures like dams or bridges. The sensor can be directly embedded into concrete and mortars or surface mounted on existing and new-built structures to measure their deformation.

Acknowledgements

The authors would like to acknowledge the Polish State Committee for Scientific Research for founding this work under grant 7 T11B 014 21.

References

1. B. Mason and T. Valis, "Commercialisation of fiber-optic strain gauge systems", *Proc. SPIE* **1795**, 215–222 (1992).
2. V. Vohra, "Fiber Bragg grating sensor for civil structure monitoring", *Proc. 13th Conf. Optical Fiber Sensors*, 32–42 (1996).
3. S. Lloret, D. Inaudi, and S. Vurppillot, "Static and dynamic monitoring with fiber optic sensors", *Proc. SPIE* **3555**, 136–146 (1998).
4. B. Lee, "Review of the present status of optical fiber sensors", *Optical Fiber Technology* **9**, 57–79 (2003).
5. J. Bush and A. Cekorich, "Commercialisation of interferometer interrogation techniques for fiber sensing applications", *Proc. 16th Conf. Optical Fiber Sensors*, (2002).
6. B. Chiu and M. Hasting, "Digital demodulation for passive homodyne optical fiber interferometry based on a 33 coupler", *Proc. SPIE* **2292**, 371–382 (1994).
7. D. Hogg, D. Janzen, T. Valis, and R. Measures, "Development of fiber Fabry-Perot strain gauge", *Proc. SPIE* **1588**, 300–307 (1991).
8. B. Culshaw and J. Dakin, *Optical Fiber Sensors*, Artech House, Boston, 1989.
9. J. Sakai and T. Kimura, "Birefringence and polarization characteristics of single-mode optical fiber under elastic deformation", *IEEE J. Quantum Electron.* **17**, 1041–1056 (1981).
10. J.W. Goodman, *Statistical Optics*, John Wiley & Sons, London, 1988.
11. M. Szustakowski and N. Palka, "Novel fiber optic contrast-based sensor", *Proc. SPIE* **5272** (2003).
12. M. Chojnacki and N. Palka, "Demodulation of output signals from unbalanced fibre optic Michelson's interferometer", *Proc. IEEE TCSET, Modern Problems of Radio Engineering, Telecommunications and Computer Science*, Slavsk, 249–250 (2002).
13. W. Demtroder, *Laser Spectroscopy. Basic Concepts and Instrumentation*, Springer-Verlag, Berlin, 1988.
14. M. Szustakowski, N. Palka, and W. Ciurapiński, "Simulations and experimental research of fiber optic contrast-based dislocation sensor", *Proc. SPIE* **5459** (2004). (in print).
15. *Guide to the Expression of Uncertainty in Measurement*, International Organization for Standardization, 1993.